SUPPORTING INFORMATION

Rapid estimation of catalytic efficiency by cumulative atomic multipole moments: application to ketosteroid isomerase mutants

Wiktor Beker[1], Marc van der Kamp[2,3,4]*, Adrian Mulholland[2,3], W. Andrzej Sokalski*[1]

[1]Advanced Materials Engineering and Modelling Group, Faculty of Chemistry, Wroclaw University of Technology, wyb. Wyspianskiego 27, 50-370 Wroclaw, Poland

[2]School of Biochemistry, Biomedical Sciences Building, University Walk, Bristol, BS8 1TD, UK

[3]BrisSynBio Synthetic Biology Research Centre, Life Sciences Building, Tyndall Avenue, University of Bristol, BS8 1TQ, UK

[4]Centre of Computational Chemistry, School of Chemistry, Cantock's Close, University of Bristol, BS8 1TS, UK.

Contents

Molecular dynamics simulations of KSI variants complexed with the intermediate state (IS)

System set-up and parameters

The protein coordinates of the KSI dimer were taken from PDB entry 1OHP, chains A and B, with Asn38 mutated back to the wild-type catalytic base Asp38. In chain A, the intermediate of the KSI reaction was included, based on the coordinates of the co-crystallised inhibitor 5α-estran-3,17-dione, whereas 5α-estran-3,17-dione was removed from the active site of chain B. Asp99 was treated as protonated in both chains (in line with its role in the enzyme and predicted pK_a values from PropKa3.1 [1] of 8.2 in chain A with the substrate bound and 9.2 in chain B with an empty active site), and Asp38 was treated as protonated only in chain A, based on the mechanism (Asp38 has abstracted the proton from C4 of the substrate to form the intermediate; see scheme in main manuscript). All other ionisable residues were treated in their standard protonation states (Asp/Glu negatively charged, Arg/Lys positively charged, His neutral). All three histidines in both chains were modeled as the tautomer protonated on Nε2 and the functional groups of the following residues were 'flipped' (rotated by 180°) as predicted by the Optimal Hydrogen Bonding Network [2]: Asn2, Asn104, His100 and His122 in chain A, and Asn19, Asn57 and Asn104 in chain B.

All crystallographic waters were kept and additional water molecules were added using the *solvate* plugin to VMD [3] (with a 'buffer' for overlapping water deletion of 2.3) such that the edge of the waterbox was at least 11 Å away from any protein atom. The *autoionize* plugin was then used to replace 6 bulk waters with Na^+ to neutralise the system. The resulting PSF file (generated by the VMD plugin *psfgen*) was converted by the AmberTools14 utility *chamber* into a prmtop file that can be used by AMBER. This ensures that CHARMM force-fields are accurately interpreted by AMBER [4]. The CHARMM36 [5] force-field was used for the protein, TIP3P [6] for water and CgenFF [7] parameters (atom types assigned using https://cgenff.paramchem.org) with CHELPG charges (obtained with the RED Server [8]) for the intermediate state. The resulting topology file is given below.

CgenFF topology file for the KSI substrate in the intermediate state, with CHELPG charges obtained through the RED Server[8]:

```
AUTO ANGLES DIHE
RESI IS1          -1.000 !
GROUP             ! CHELPG charges
ATOM C1     CG321     -0.0333
ATOM H1A    HGA2      -0.0210
ATOM H1B    HGA2      -0.0210
ATOM C2     CG321     -0.1135
ATOM H2A    HGA2      0.0105
ATOM H2B    HGA2      0.0105
ATOM C3     CG2D1O    0.6927
ATOM O3     OG312     -0.8009
ATOM C4     CG2DC1    -0.8064
ATOM H4B    HGA4      0.1680
ATOM C5     CG2DC2    0.2701
ATOM C6     CG2DC2    -0.6545
```

```
ATOM H6A    HGA4     0.1585
ATOM C7     CG321    0.2989
ATOM H7A    HGA2     -0.0719
ATOM H7B    HGA2     -0.0719
ATOM C8     CG311    0.0312
ATOM H8A    HGA1     -0.0308
ATOM C9     CG311    0.0218
ATOM H9A    HGA1     -0.0559
ATOM C10    CG301    0.2475
ATOM C19    CG331    -0.1532
ATOM H13A   HGA3     0.0118
ATOM H13B   HGA3     0.0118
ATOM H13C   HGA3     0.0118
ATOM C11    CG321    0.1238
ATOM H11A   HGA2     -0.0405
ATOM H11B   HGA2     -0.0405
ATOM C12    CG321    -0.1188
ATOM H12A   HGA2     0.0000
ATOM H12B   HGA2     0.0000
ATOM C13    CG3RC1   0.2651
ATOM C18    CG331    -0.2838
ATOM H18A   HGA3     0.0576
ATOM H18B   HGA3     0.0576
ATOM H18C   HGA3     0.0576
ATOM C14    CG3RC1   -0.0088
ATOM H14A   HGA1     -0.0113
ATOM C15    CG3C52   -0.0483
ATOM H15A   HGA2     0.0043
ATOM H15B   HGA2     0.0043
ATOM C16    CG3C52   -0.1361
ATOM H16A   HGA2     0.0431
ATOM H16B   HGA2     0.0431
ATOM C17    CG2O5    0.5131
ATOM O17    OG2D3    -0.5923
BOND C1   H1A
BOND C1   H1B
BOND C1   C2
BOND C1   C10
BOND C2   H2A
BOND C2   H2B
BOND C2   C3
BOND C3   O3
BOND C3   C4
BOND C4   H4B
BOND C4   C5
BOND C5   C6
BOND C5   C10
BOND C6   H6A
BOND C6   C7
BOND C7   H7A
BOND C7   H7B
BOND C7   C8
```

```
BOND C8   H8A
BOND C8   C9
BOND C8   C14
BOND C9   H9A
BOND C9   C10
BOND C9   C11
BOND C10  C19
BOND C19  H13A
BOND C19  H13B
BOND C19  H13C
BOND C11  H11A
BOND C11  H11B
BOND C11  C12
BOND C12  H12A
BOND C12  H12B
BOND C12  C13
BOND C13  C18
BOND C13  C14
BOND C13  C17
BOND C18  H18A
BOND C18  H18B
BOND C18  H18C
BOND C14  H14A
BOND C14  C15
BOND C15  H15A
BOND C15  H15B
BOND C15  C16
BOND C16  H16A
BOND C16  H16B
BOND C16  C17
BOND C17  O17
IMPR C17    C16    C13    O17
```

Simulation and analysis - methods

All simulations were performed with the AMBER package v. 14. Two independent simulations were performed for each mutant (with randomized positions of the Na^+ ions prior to initial minimisation).

Minimisations were performed with sander (on single CPUs) and MD simulations with pmemd.MPI (on 8 CPUs). Each system was prepared for MD simulation by initial minimisation of all solvent, the substrate and all hydrogens (300 steps), a brief (50 ps) MD simulation of all solvent and finally a minimisation of all atoms (300 steps) with positional restraints on the protein Cα atoms of 5.0 kcal mol^{-1} $Å^{-2}$. The system was then heated (after random assignment of velocities at 25 K) to 298 K in 20 ps, using Langevin dynamics for temperature control (collision frequency of 1 ps), again with the positional restraints on the protein Cα atoms. The positional restraints were gradually released and the pressure equilibrated to 1 atm in 4 steps of 10 ps, using the Berendsen barostat (pressure relaxation time 1 ps). Finally, 1 ns simulations were performed in the NPT ensemble at 298 K and 1 atm (with Langevin dynamics for temperature control and the Berendsen barostat). Throughout all MD simulations, a one-sided restraint was applied to ensure that the distance between Asp38 Oδ2 and C4 of the substrate does not become larger than 2.65 Å, so that the conformations sampled are in line with the reaction mechanism. Further, a 2

fs timestep was used with SHAKE applied to bonds involving hydrogen, the cut-off for direct-space non-bonded interactions was 8 Å and long-range electrostatics were treated using the Particle Mesh Ewald method.
The 2 trajectories obtained from two 1 ns simulations (saved every 1 ps) were clustered based on the mass-weighted RMSD of the substrate, Asp38 (the catalytic base) and the residues at positions 14 & 99 in chain A. The hierarchical agglomerative algorithm was used and 4 clusters were requested, using the AmberTools program cpptraj [9].

Convergence of Differential Intermediate State Stabilization (DISS) energy calculated by Cumulative Atomic Multipole Moments (CAMM)

To test whether the multipolar expansion of the differential intermediate state stabilization (DISS) in KSI converges, calculations were performed at different truncation levels L ($L=L_a+L_b$, the sum of ranks of multipole moments of monomer a and b, related to the inverse distance term in the multipole expansion via $R^{-(L+1)}$ (exponent truncation), see ref. [10]). Calculations were performed for all KSI variants considered (Figures S1-S5), employing the whole (rather than the truncated) substrate (see Figure 3) and structures obtained with the minimal perturbation approach (see main text). The CAMM expansion of the DISS energy is close to convergence after the R^{-4} term (L=3) in most cases. Results diverge after R^{-6} or R^{-7} (L=5 or 6, respectively) in some cases, which is likely related to numerical errors in the determination of high-rank; see also further discussion in the main text. Overall, the truncation level R^{-5} (L=4) is a reasonable choice.

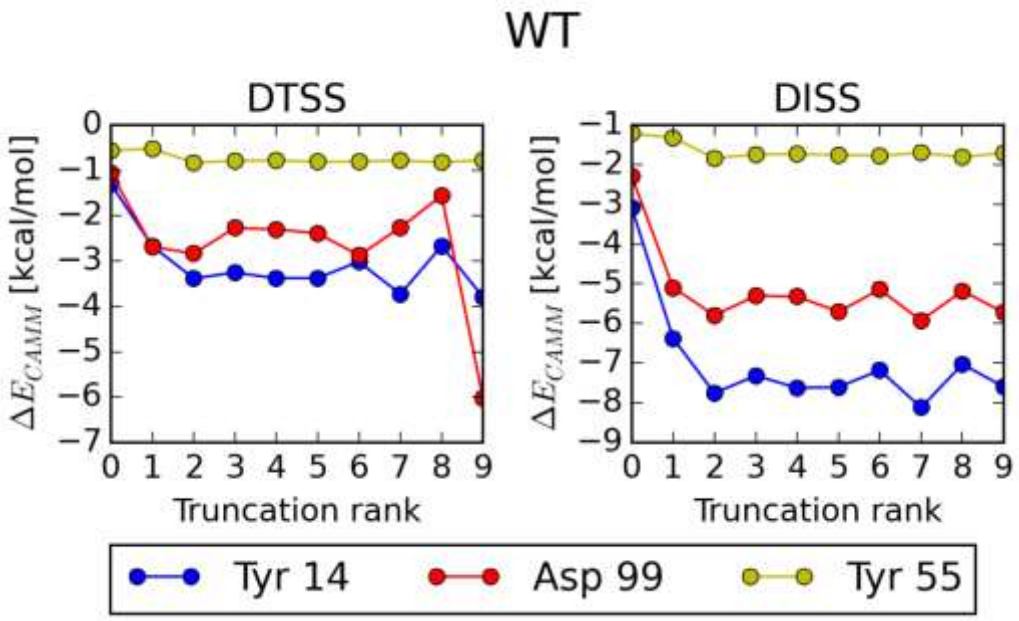

Figure S1. Convergence of CAMM DISS and DTSS energy in wild-type KSI (QM/MM structure from ref. [11]). The multipolar contribution to the differential intermediate state stabilization as calculated with various truncation levels of CAMM expansion.

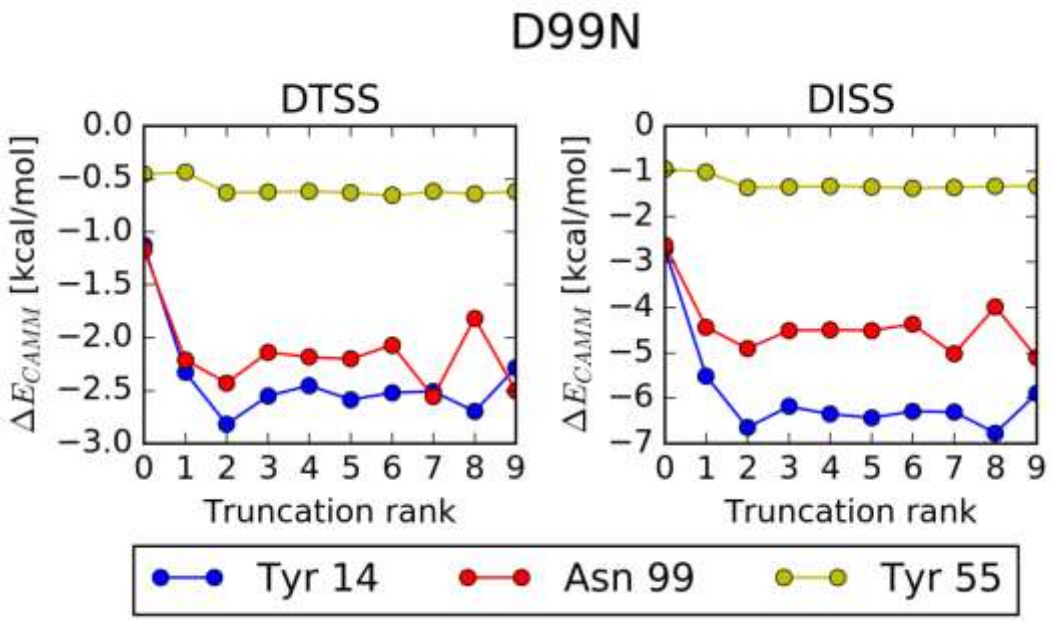

Figure S2. Convergence of CAMM DISS and DTSS energy in the D99N KSI mutant. The multipolar contribution to differential intermediate state stabilization calculated with various truncation levels of CAMM expansion.

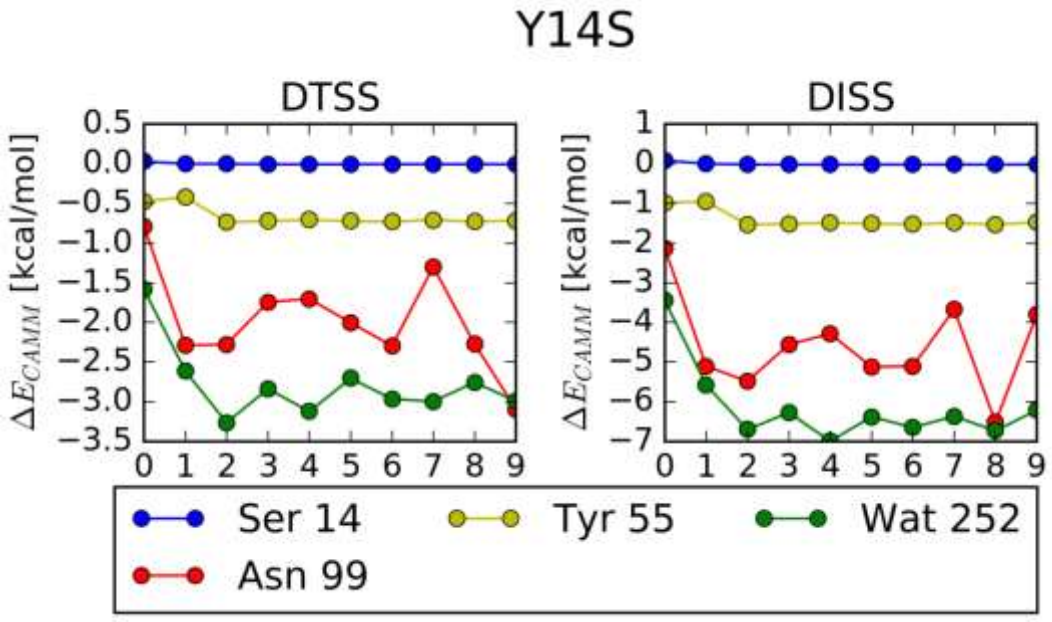

Figure S3. Convergence of CAMM DISS and DTSS energy in the Y14S KSI mutant. The multipolar contribution to differential intermediate state stabilization calculated with various truncation levels of CAMM expansion.

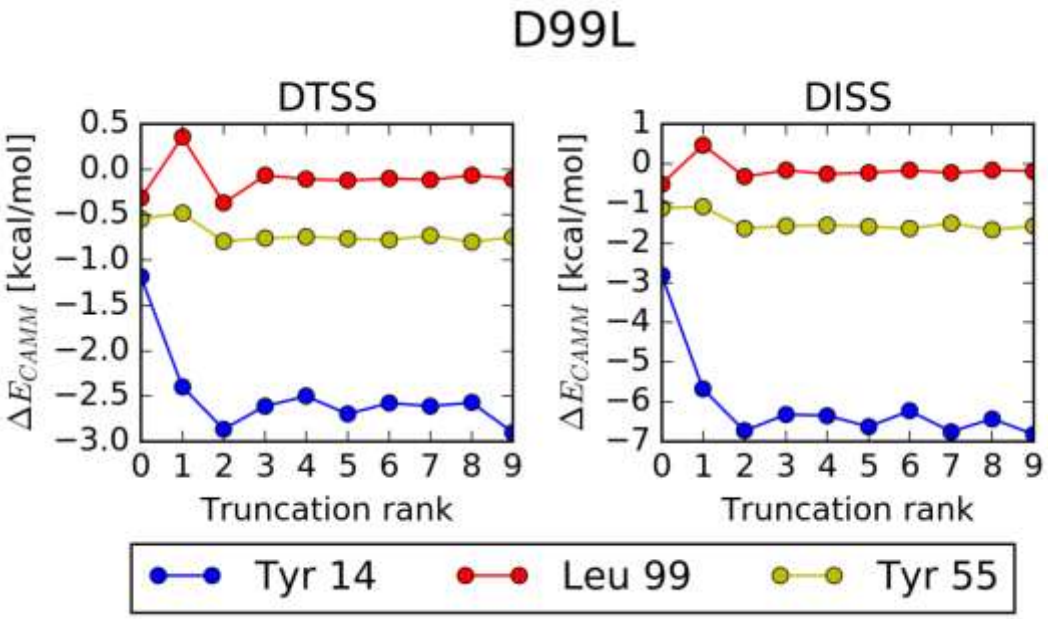

Figure S4. Convergence of CAMM DISS and DTSS energy in the D99L KSI mutant. The multipolar contribution to differential intermediate state stabilization calculated with various truncation levels of CAMM expansion.

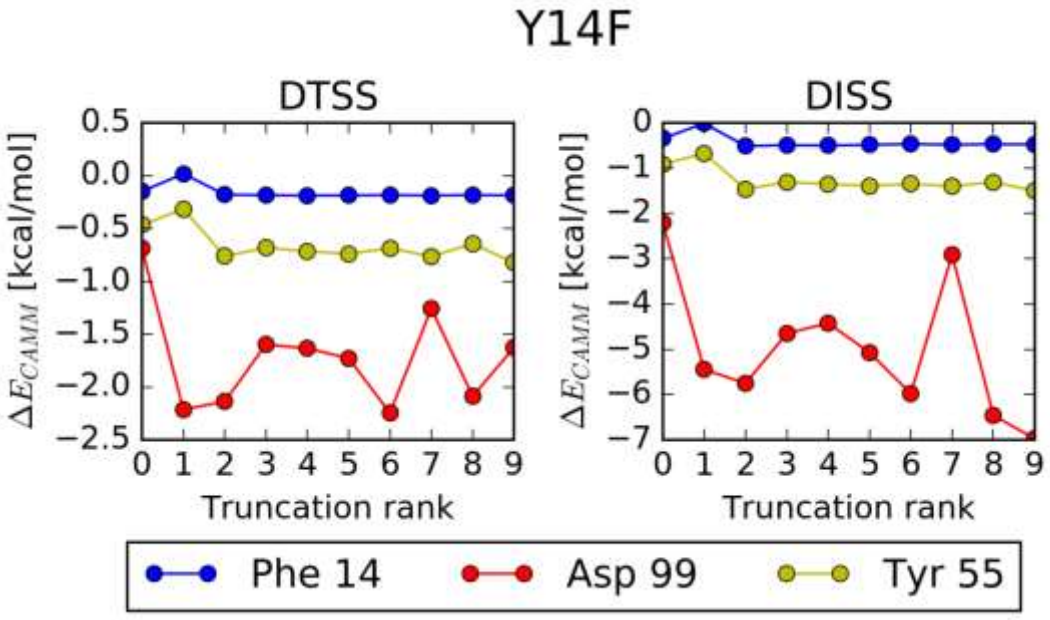

Figure S5. Convergence of CAMM DISS and DTSS energy in the Y14F KSI mutant. The multipolar contribution to differential intermediate state stabilization calculated with various truncation levels of CAMM expansion.

Linear regression parameters

Table S1. Best-fit parameters, Pearson correlation coefficients (ρ_P) and Spearmann rank correlation coefficients (ρ_S) between differential intermediate state stabilization (DISS) and experimental apparent free energy barriers (calculated from the works of Kraut and Choi[12,13], see Computational details). Calculations are based on the cluster centroid structures obtained from MD simulation (see Computational details).

MD clusters

	All mutants				Without Y14S			
Method	slope	intercept	ρ_P	ρ_S	slope	intercept	ρ_P	ρ_S
$\Delta E_{MTP}^{(10)}(CAMM)$	0.47 ± 0.12	17.9 ± 1.2	0.92	0.9	0.53 ± 0.08	18.21 ± 0.71	0.98	1.0
$\Delta E_{elst}^{(10)}$	0.37 ± 0.09	18.0 ± 1.2	0.93	0.9	0.41 ± 0.08	18.21 ± 0.9	0.97	1.0
ΔE_{HF}	0.50 ± 0.12	20.3 ± 1.7	0.93	1.0	0.56 ± 0.09	20.7 ± 1.2	0.98	1.0
ΔE_{SAPT0}	0.5 ± 0.1	20.2 ± 1.5	0.94	1.0	0.51 ± 0.08	20.5 ± 1.2	0.98	1.0

Table S2. Best-fit parameters, Pearson correlation coefficients (ρ_P) and Spearmann rank correlation coefficients (ρ_S) between differential intermediate state stabilization (DISS) and experimental apparent free energy barriers (calculated from the works of Kraut and Choi[12,13], see Computational details). Calculations are based on the 'minimal perturbation' structures (see Computational details).

Minimal Perturbation Structures

	All mutants				Without Y14S			
Method	slope	intercept	ρ_P	ρ_S	slope	intercept	ρ_P	ρ_S
$\Delta E_{MTP}^{(10)}(CAMM)$	0.52 ± 0.12	18.8 ± 1.2	0.94	1.0	0.57 ± 0.06	19.0 ± 0.6	0.99	1.0
$\Delta E_{elst}^{(10)}$	0.32 ± 0.15	18.5 ± 2.4	0.78	0.3	0.32 ± 0.19	18.0 ± 3.0	0.78	0.2
ΔE_{HF}	0.4 ± 0.1	19.3 ± 1.4	0.94	1.0	0.45 ± 0.12	19.3 ± 1.6	0.94	1.0
ΔE_{SAPT0}	0.48 ± 0.06	20.4 ± 0.9	0.98	1.0	0.48 ± 0.07	20.4 ± 1.1	0.98	1.0

Comparison of DISS obtained with CAMM or with fixed point charges

Here, we compare the use of CAMM with the use of a fixed point charge model for calculating Differential Intermediate State Stabilization for KSI variants. Point charges were CHELPG charges as obtained with the RED Server [8] for the reactant and intermediate states. Both approaches have a similar trend, but it should be noted that the point-charge approach benefits from a significant cancellation of errors (Table S3); Note that DISS (defined as $E_{int}(IS) - E_{int}(RS)$) is dominated by the interaction energy with the intermediate state, which in turn is quite well described by a point charge model (due to its non-zero charge). This is reflected in the fact that the difference between the point charge (FF) and CAMM interaction energies is small this state (compared to the reactant state). The errors in interaction energies of the point charge model (compared to the CAMM model) are not systematic, indicating that changing the point charges used cannot easily improve the results.

Table S3. Comparison of CAMM and FF charges energies ('Minimal perturbation' structure)

MUTANT	CAMM RS [kcal/mol]	FF RS [kcal/mol]	δ RS [kcal/mol]	CAMM IS [kcal/mol]	FF IS [kcal/mol]	δ IS [kcal/mol]	CAMM DISS [kcal/mol]	FF DISS [kcal/mol]	δ DISS [kcal/mol]
WT	−23.15	−18.95	4.20	−36.24	−34.35	1.89	−13.09	−15.40	−2.31
D99N	−20.55	−16.11	4.44	−32.87	−30.92	1.95	−12.32	−14.80	−2.48
Y14S	−22.28	−18.07	4.21	−34.07	−31.50	2.57	−11.79	−13.44	−1.64
D99L	−14.48	−12.18	2.30	−22.42	−21.11	1.31	−7.94	−8.93	−0.99
Y14F	−13.29	−11.10	2.18	−19.03	−18.58	0.45	−5.74	−7.47	−1.73
R	0.86	0.85		0.90	0.91		0.94	0.94	
$R_{(noY14S)}$	0.96	0.96		0.98	0.97		0.99	0.97	

For both models (CAMM and force field point charges FF), interaction energies with substrate (RS) and intermediate (IS) are shown, as well as their difference (Differential Intermediate Stabilization, DISS) and the deviation of the point charge model from CAMM (δs) for all the values. For interaction energies, Pearson correlation coefficients (*R*) with experimental apparent free energy barriers (calculated from the works of Kraut and Choi[12,13], see Computational details) are given, with and without inclusion of Y14S ($R_{(no\ Y14S)}$).

Further comparison of CAMM with point charge approximations is provided in Figure S6. Here, we consider reactants and Asp99; by increasing the separation between their centers of mass, we monitor Asp99 contribution to the DISS as a function of distance difference DX (with respect to the value from QM/MM study). As a reference we took the DMA multipole moments[14]. The results indicate that point charge models cannot reproduce charge anisotropy well in comparison to CAMM.

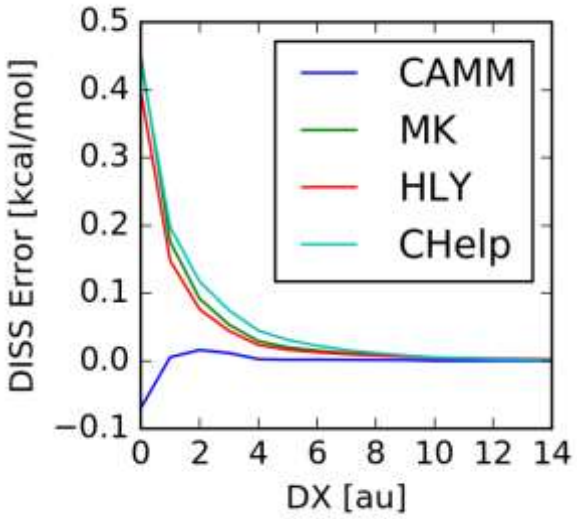

Figure S6. Error in DISS contribution of Asp 99 as a function of the separation with respect to the value from the QM/MM study. DMA multipoles serve as a reference. CAMM- Cumulative Atomic multipole moments (up to R^{-5}); MK-Merz-Singh-Kollman[15,16], HLY-Hu,Lu,Yang[17], CHelpG[18]. DX- distance by which the separation of centers of mass is varied; zero value corresponds to equilibrium geometry.

Comparison with Chakravorty and Hammes-Schiffer (Biochemistry, 2009)

Table S4. Comparison of intermediate stabilization energies (all in kcal/mol) between Chakravorty and Hammes-Shiffer's work[19] and the present study. Apparent activation barriers calculated basing on experimental data from Kraut and Choi[12,13] (see *Computational details*).

Enzyme	$\Delta G_{app}^{\ddagger}$ [12,13]	E_{EL}(RS)[19]	E_{EL}(IS)[19]	E_{EL}(IS)-E_{EL}(RS)	DISS(CAMM)
WT	11.5	-30	-101	-71	-15
D99L	14.2	-24	-84	-60	-8
Y14F	16.0	-27	-91	-64	-6

The differences between Chakravorty and Hammes-Shiffer's work[19] and our work arise mainly from different sizes of system used in both set of calculations (in our work, the Asp38 side-chain was included in the system considered for the interaction energy calculations, in contrast to Chakravorty and Hammes-Shiffer's work**)**. However, applying our approach to point-charge model of whole proteins leads to values consistent with presented CAMM results and of magnitudes comparable to those from EVB study[19] (see Table S5). There are also minor technical differences impeding direct numerical comparison of these two approaches. Firstly, different PDB structures where used as a starting point for modeling (PDB code 1QJG in EVB study and 1OHP here).

Table S5. Interaction energies (in kcal/mol) between androstedione and its environment calculated with point charges (structures obtained from clustering of MD simulations). The values are similar to those presented in Table S4 in the work of Chakravorty and Hammes-Schiffer[19].

Protein	**E_{EL}(RS)**	**E_{EL}(IS)**	**E_{EL}(IS)- E_{EL}(RS)**
WT	-42	-126	-84
D99N	-45	-123	-78
Y14S	-46	-133	-87
D99L	-40	-120	-80
Y14F	-42	-126	-84

Testing the importance of many-body polarization

To examine the three-body effects associated with polarization, we chose the Tyr14-Tyr55 interaction as a test-case. The hydrogen bond donated by Tyr55 to the Tyr14 –OH may polarize this group and thus strengthen its O-H dipole. To include this effect, the wavefunction was calculated for both residues treated as one system and used for the determination of CAMMs. Subsequently, DISS calculations with this polarized Tyr14 system were compared with DISS calculations using including the individual, non-polarized tyrosine residues (Table S6). In case of the Y14S and Y14F mutants, the same strategy was applied, including Ser14,W_{TyrOH} and Tyr55 in the former, and Phe14 and Tyr55 in the latter case. All three variants that contain the Tyr14-Tyr55 system show a similar influence of polarization: the differential stabilization decreases (i.e. stronger relative stabilization of the intermediate state) by about 0.5 kcal/mol compared to the non-polarized model. Thus, the error arising from the neglecting Tyr14-Tyr55 polarization is ~7% of the 'polarized' value. It is further found that the Tyr55 contribution is nearly constant among mutants (~ −1.5 kcal/mol) and we expect similar behavior from other residues common in all considered variants.

In Y14F, the polarization effect of Tyr55 *increases* the DISS (i.e. weaker relative stabilization of the intermediate state compared to the reactant state); it's worth noting that in this mutant, the value presented in Table S6 is dominated by Tyr55 (−1.35 kcal/mol). On the other hand, in Y14S the difference is large in comparison with other variants (about 1.2 kcal/mol). This mutation is more difficult to model using the DISS(CAMM) approach (see discussion in main text).

Table S6. Comparison of DISS energies (in kcal/mol) calculated using a non-polarized (per-residue) CAMM model and one that includes explicit residue 55 – residue 14 polarization.

Mutant	Residues polarized	Residues unpolarized	Difference (pol.-unpol.)
WT	-10.02	-9.35	-0.67
D99N	-8.10	-7.68	-0.42
Y14S	-9.70	-8.51	-1.20
D99L	-8.40	-7.89	-0.50
Y14F	-1.63	-1.85	0.23

The influence of structure on SAPT results and mutual cancelling of interaction energy terms

In the main text, it was shown that the difference between DISS(CAMM) energies obtained for Minimal Perturbation (MP) structures and MD cluster centroids (MD) is small or at least nearly systematic. Here we present a similar comparison for other terms as defined by SAPT (Figure S7). The most dramatic case is the D99L mutant, where the short-range penetration term is responsible for overestimation of Leu99 electrostatic ($\Delta E_{EL}^{(10)}$) contribution. Other levels (ΔE_{HF} and ΔE_{SAPT0}) are less affected by the structural change by mutual cancelling of those short-range terms (see Figure S8). However, this change is larger and less systematic than that observed in CAMM (see main text).

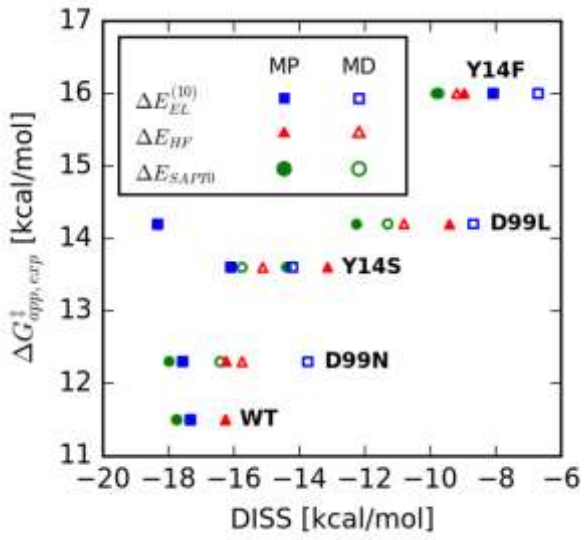

Figure S7. DISS energies calculated with different levels in SAPT decomposition, using 'minimal perturbation' (MP) structures and MD trajectory cluster centroids (MD).

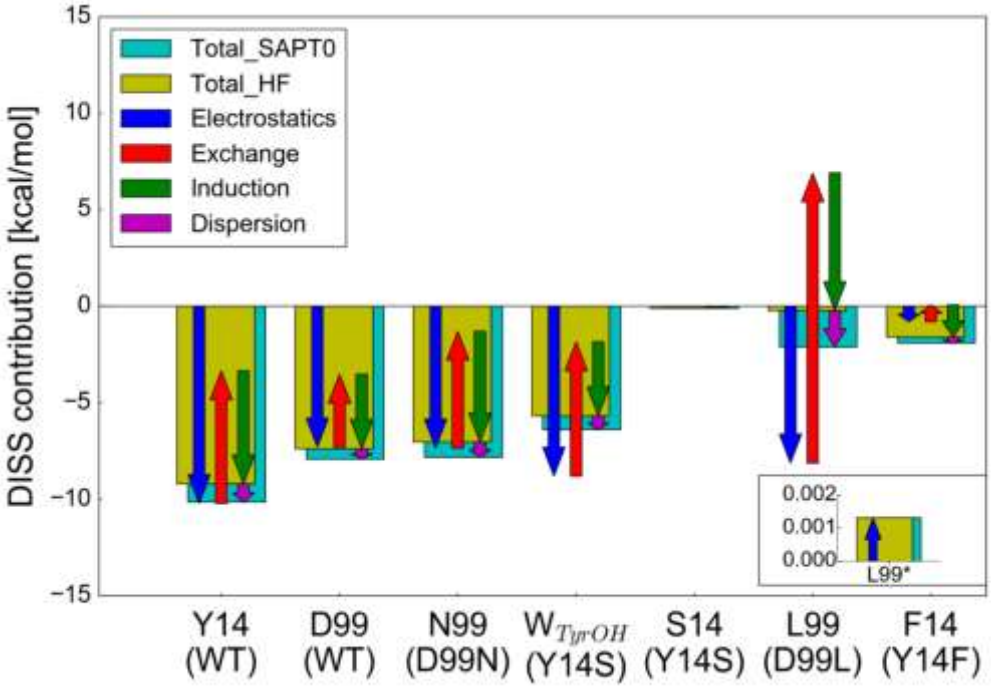

Figure S8. A decomposition of DISS contribution arising from analyzed amino acids (in Minimal Perturbation geometries). Subsequent contributions (according to SAPT[20] decomposition) are marked as arrows and aligned head-to-tail.

The effect of substrate truncation

We provide details of comparison between results obtained with full substrate and the one truncated to the two rings encompassing atoms participating in reaction (see Computational Details in main text). As can be seen in Table S7, the maximum error is smaller than 0.5 kcal/mol for overall DISS, with errors for DISS calculated with CAMM are the lowest (<0.25 kcal/mol).

Table S7. DISS error arising from truncation of the substrate ($DISS_{whole}$-$DISS_{truncated}$, kcal/mol).

	Tyr 14	Asp 99	Tyr 55	Sum
$\Delta E_{MTP}^{(10)}(CAMM)$	0.06	0.09	0.10	0.24
$\Delta E_{elst}^{(10)}$	0.06	0.13	0.09	0.27
ΔE_{HF}	0.16	0.15	0.11	0.43
ΔE_{SAPT0}	0.15	0.15	0.11	0.41

Comparison of computational requirements of CAMM, HF and SAPT0 calculations

To indicate the difference in computational effort of CAMM, HF(SCF) and SAPT0 calculations, we compare the computer times required for evaluation of electrostatic interaction energies for homodimers within S22 training set[21], see Figure S9. (Hereafter, *A* and *N* state for number of atoms and basis set functions in monomers, respectively.) Note that CAMM(R^{-5}) calculations for this training set take only a few miliseconds, scaling approximately as O(A^2), a negligible value compared to the SAPT0 electrostatic term evaluation in the dimer basis set, scaling as O($(2N)^4$) . It should be mentioned that CAMM energy calculations of any new chemical species requires two SCF runs for each monomer, each one scaling as O(N^4), to determine multipole moments (see the SCF series in Fig. S9). However, with a library of pre-computed CAMMs for aminoacids and one initial SCF calculation for each ligand/transition state, evaluation of interaction energies with any number of amino acid residues (including e.g. different enzyme variants) will follow the CAMM curve rather than the SCF curve presented in Fig. S9.

All times presented in Figure S9 were evaluated using the same machine, containing two Intel® Xeon® E5-2630 v2 @ 2.60 GHz CPUs. SCF for monomers from S22 training set[21] were obtained using GAMESS[22] with 12 threads, whereas SAPT0 energies were calculated with PSI4[23], using the same number of threads. All computations were done with aug-cc-pVDZ basis set.

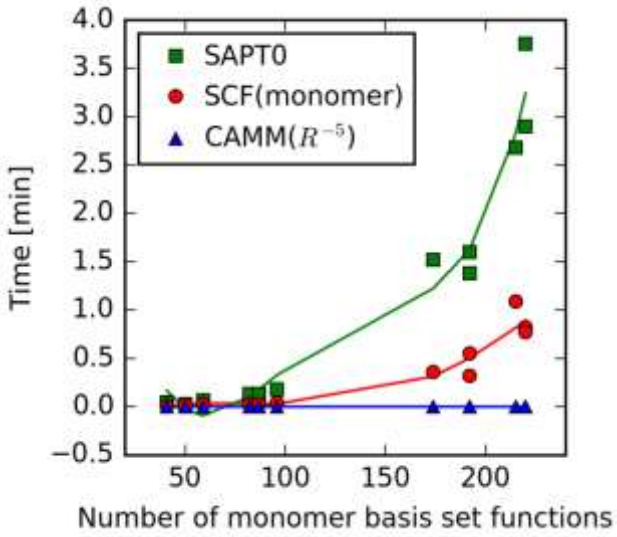

Figure S9. Comparison of computational times of evaluation of CAMM and SAPT0 energies in homodimers from S22 training set[21]. System size is measured as total number of basis set functions in dimer. Here, SCF series mean total time required to determine CAMMs for each monomer. Note that sole CAMM interaction energy calculation takes a few milliseconds.

REFERENCES

(1) Sondergaard, C. R.; Olsson, M. H. M.; Rostkowski, M.; Jensen, J. H. *J. Chem. Theory Comput.* **2011**, *7* (7), 2284–2295.

(2) Hooft, R. W. W.; Sander, C.; Vriend, G. *Proteins* **1996**, *26*, 363–376.

(3) Humphrey, W.; Dalke, A.; Schulten, K. *J. Mol. Graph.* **1996**, *14*, 33–38.

(4) Crowley, M. F.; Williamson, M. J.; Walker, R. C. *Int. J. Quantum Chem.,* **2009**, *109*, 3767–3772.

(5) Best, R. B.; Zhu, X.; Shim, J.; Lopes, P. E. M.; Mittal, J.; Feig, M.; MacKerell Jr., A. D. *J. Chem. Theory Comput.* **2012**, No. 8, 3257–3273.

(6) Jorgensen, W. L.; Chandrasekhar, J.; Madura, J. D.; Impey, R. W.; Klein, M. L. *J. Chem. Phys.* **1983**, *79*, 926.

(7) Vanommeslaeghe, K.; Hatcher, E.; Acharya, C.; Kundu, S.; Zhong, S.; Shim, J.; Darian, E.; Guvench, O.; Lopes, P.; Vorobyov, I.; MacKerell Jr., A. D. *J. Comput.*

Chem. **2010**, *31*, 671–690.

(8) Vanquelef, E.; Simon, S.; Marquant, G.; Garcia, E.; Klimerak, G.; Delepine, J. C.; Cieplak, P.; Dupradeau, F. Y. *Nucleic Acids Res.* **2011**, *39*, W511–W517.

(9) Roe, D. R.; Cheatham, T. E. I. *J. Chem. Theory Comput.* **2013**, *9* (7), 3084–3095.

(10) Sokalski, W. A.; Poirier, R. A. *Chem. Phys. Lett.* **1983**, *98* (1), 86–92.

(11) van der Kamp, M. W.; Chaudret, R.; Mulholland, A. J. *Febs J.* **2013**, *280* (13), 3120–3131.

(12) Kraut, D. A.; Sigala, P. A.; Fenn, T. D.; Herschlag, D. *Proc. Natl. Acad. Sci. U. S. A.* **2010**, *107* (5), 1960–1965.

(13) Choi, G.; Ha, N. C.; Kim, M. S.; Hong, B. H.; Oh, B. H.; Choi, K. Y. *Biochemistry* **2001**, *40* (23), 6828–6835.

(14) Stone, A. J. *Chem. Phys. Lett.* **1981**, *83* (2), 233.

(15) Besler, B. H.; Merz, K. M. J.; Kollman, P. A. *J. Comput. Chem.* **1990**, *11*, 431–439.

(16) Singh, U. C.; Kollman, P. A. *J. Comput. Chem.* **1984**, *5*, 129–145.

(17) Hu, H.; Lu, Z.; Yang, W. *J. Comput. Chem.* **2007**, *3*, 1004–1013.

(18) Chirlian, L. E.; Francl, M. M. *J. Comput. Chem.* **1987**, *8*, 894–905.

(19) Chakravorty, D. K.; Soudackov, A. V; Hammes-Schiffer, S. *Biochemistry* **2009**, *48* (44), 10608–10619.

(20) Cwiok, T.; Jeziorski, B.; Kolos, W.; Moszynski, R.; Szalewicz, K. *Theochem-Journal Mol. Struct.* **1994**, *113*, 135–151.

(21) Jurecka, P.; Sponer, J.; Cerny, J.; Hobza, P. *Phys. Chem. Chem. Phys.* **2006**, *8* (17), 1985–1993.

(22) Schmidt, M. W.; Baldridge, K. K.; Boatz, J. A.; Elbert, S. T.; Gordon, M. S.; Jensen, J. H.; Koseki, S.; Matsunaga, N.; Nguyen, K. A.; Su, S. J.; Windus, T. L.; Dupuis, M.; Montgomery, J. A. *J. Comput. Chem.* **1993**, *14* (11), 1347–1363.

(23) Turney, J. M.; Simmonett, A. C.; Parrish, R. M.; Hohenstein, E. G.; Evangelista, F. A.; Fermann, J. T.; Mintz, B. J.; Burns, L. A.; Wilke, J. J.; Abrams, M. L.; Russ, N. J.; Leininger, M. L.; Janssen, C. L.; Seidl, E. T.; Allen, W. D.; Schaefer, H. F.; King, R. A.; Valeev, E. F.; Sherrill, C. D.; Crawford, T. D. *Wiley Interdiscip. Rev. Mol. Sci.* **2012**, *2* (4), 556–565.